



# Scatter Compensation Techniques in PET

Habib Zaidi, PhD, PD\*, Marie-Louise Montandon, PhD

- |   |   |
|---|---|
| <ul style="list-style-type: none"> <li>■ What is Compton scatter?</li> <li>■ Practical and clinical consequences of scatter detection</li> <li>■ Modeling the scatter component in uniform and non-uniform media</li> <li>■ Scatter component in small-animal positron emission tomography imaging</li> <li>■ Scatter-correction strategies in positron emission tomography<br/><i>Hardware approaches using coarse septa or beam stoppers</i></li> </ul> | <ul style="list-style-type: none"> <li><i>Multiple-energy-window (spectral) approaches</i></li> <li><i>Approaches based on convolution or deconvolution</i></li> <li><i>Approaches based on direct calculation of scatter distribution</i></li> <li><i>Iterative reconstruction-based scatter-correction approaches</i></li> <li><i>Comparison of methods</i></li> <li>■ Scatter correction in transmission imaging</li> <li>■ Summary</li> <li>■ References</li> </ul> |
|---|---|

In PET scatter detection usually refers to Compton scattering in which one or both annihilation photons undergo an interaction with matter (eg, the patient), changing direction and losing energy. The scattering angle is closely related to the energy transferred to the electron, so that the energy loss approaches zero when the change in direction approaches zero. Because of its small contribution to the total cross section for PET energies, coherent scattering is often overlooked [1]. The detected scattered photons falling within the energy acquisition window (eg, 350–650 kilo electron volts [keV]) are those for which one wishes compensation. Usually, annihilation photons can scatter in the patient and in material outside the patient (eg, the bed supporting the patient, the detector material, the electronics behind the detector, or anywhere within the gantry). This article focuses on scattering within the patient, because the magnitude of other scatterings

probably is small enough to justify ignoring them. One should keep in mind that multiple scatter detection might occur in two or more places in the same object. When developing and implementing a scatter-compensation method, one should be aware of which types of scatter are expected and are being corrected.

The rationale behind scatter compensation generally is to enhance the contrast of reconstructed PET images, to improve the accuracy of activity quantification, or both. The final goal may guide the choice of the technique. Whereas it is well acknowledged that Compton scatter degrades image quality by substantially reducing the contrast, many nuclear medicine physicians and clinicians are puzzled by the clinical relevance of this image-degrading factor that is inherent to the modality. Among the frequently asked questions are the degree to which scatter detection affects

This work was supported by the Swiss National Science Foundation under grant SNSF 3100A0-116547. Division of Nuclear Medicine, Geneva University Hospital, CH-1211 Geneva, Switzerland

\* Corresponding author.

E-mail address: [habib.zaidi@hcuge.ch](mailto:habib.zaidi@hcuge.ch) (H. Zaidi).

image interpretation and clinical diagnosis, whether it affects diagnostic accuracy, and what is the real added value of scatter compensation in clinical PET imaging. Although these issues are difficult to elucidate, physicists are deeply convinced that scatter correction is a vital component in producing high-resolution, artifact-free quantitative images [2]. It is, however, their duty to debate the important issues related to design aspects of PET technology (eg, the need for scintillation crystals with improved energy resolution for better scatter discrimination) and optimal data acquisition and processing protocols, with the aim of improving image quality and obtaining accurate quantitative measures through efficient scatter removal [3,4].

Thorough reviews of scatter modeling and correction strategies in nuclear medicine imaging were published in 1994 [5] and 2004 [2]. This article addresses this issue from a different perspective: it focuses on scatter modeling and correction in fully three-dimensional (3D) PET imaging with special emphasis on most recent developments in the field in general and the most promising approaches in particular. Because of the widespread interest in both preclinical and dual-modality PET/CT imaging instrumentation, the problem of scatter detection in small-animal PET and transmission imaging is discussed also.

### What is Compton scatter?

In Compton scattering, the photon interacts with an atomic electron and is scattered through an angle  $\theta$  relative to its incoming direction, carrying less energy than it had originally (Fig. 1A). Only a fraction of the initial photon energy is transferred to the electron. After Compton (or incoherent) scattering, the scattered photon energy  $E_s$  is given by the following equation:

$$E_s = \frac{E}{1 + \frac{E}{m_0 c^2} (1 - \cos\theta)}$$

where  $E$  is the energy of the incident photon,  $m_0$  is the rest mass energy of the electron, and  $c$  is the speed of light. This equation is derived on the assumption that an elastic collision occurs between the photon and the electron, and that the electron is initially free and at rest. It is obvious from this equation that the maximum energy transfer takes place when the photon is back-scattered  $180^\circ$  relative to its incoming direction and that the relative energy transfer from the photon to the electron increases for increasing photon energies. This equation is plotted in Fig. 1B for 511 keV photons and illustrates that rather large angular deviations occur for a relatively small energy loss. There are corrections to that equation that take into account the fact that the electron actually is moving and is bound to an atom. The result is that the photons

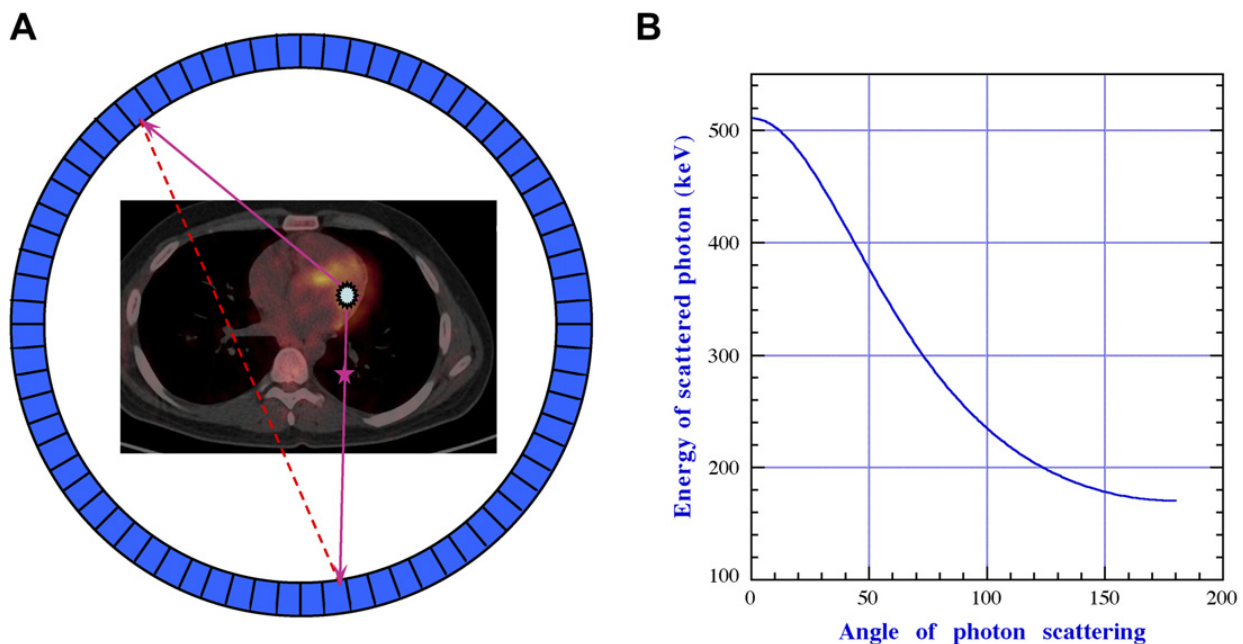


**Fig. 1.** (A) Compton scatter detection in PET. In Compton scattering a photon undergoes an interaction within the patient's body whereby it changes direction and loses energy. In single-photon emission CT neither scattered nor unscattered LoRs can be formed outside the body. In PET, scattered LoRs can be formed outside the body, but unscattered LoRs cannot. (B) The residual energy of a 511-keV incoming photon after Compton scattering through a given angle.

that are scattered through a given angle actually have a distribution of energies sharply peaked about the value calculated by the simple formula [6]. Although this effect, which is called “Doppler broadening,” has some importance for Compton cameras [7], its impact in PET is limited because the energy distribution is peaked so sharply.

Two additional issues are worth mentioning in the context of PET imaging. The first is that the loss of energy can lead to the removal of a Compton-scattered photon by the lower-level discrimination threshold set for data acquisition. Events falling outside the energy window are no longer of importance for scatter correction. The second is that the change of direction is the fundamental reason the problem needs correction, because a wrong line of response (LoR) will be assigned to this event. As a result, the recorded coincidence event is tracked back incorrectly during reconstruction, if it is assumed to be from an emission site.

Detected Compton-scattered photons may scatter only once or multiple times (two or more scatters) in the patient, the PET scanner’s gantry, or table that supports the patient. In addition, the incoming photon may originate from outside the field of view (FoV) of the scanner (out-of-FoV scatter). Earlier implementations of scatter-correction algorithms ignored both these possibilities, thus opening the opportunity to address them separately as additional effects that led to bias in the corrected estimate. “Bias” is a statistical term defined as a deviation (either up or down) in the estimated count density of the reconstructed image as compared with the true count density. These issues, however, have been considered in the more recently developed and more advanced correction procedures.

### Practical and clinical consequences of scatter detection

In the earliest literature on the deleterious effect of scatter detection, the major consequence of scatter was judged to be a loss of contrast in reconstructed PET images. In addition to a decrease in the image contrast, events also may appear in regions of the image where there is no activity (eg, outside the patient). In the most straightforward depiction, a true zero count density in a reconstructed image occurs as a positive value. This effect was demonstrated in the 1970s by imaging a line source in air and then in a water-filled bucket (see Fig. 3.22 in [8]) and by imaging nonradioactive spheres in a radioactive background [9]. The corruption commonly was portrayed as a pedestal on which the true image sat. Later, imaging scientists realized the complexity of artifacts resulting from Compton scatter detection that affect visual interpretation in at least parts

of the image and impinge on the accuracy of quantitative analysis of PET data. Consequently, Compton scatter was recognized as a non-negligible physical degrading factor, because in most situations an accurate quantitative image with the best possible contrast possible is desirable. The extent to which scatter can be shown to interfere with the purpose for which the image is to be used (eg, clinical diagnosis or outcome of studies) is a complicated issue and should be addressed through further research [10].

In radionuclide imaging, Compton scatter is the companion of photon attenuation, in that a substantial portion of the photons that are attenuated directly drop into the class of potential scatter-corrupting photons [2]. For PET energies, the interaction cross section of photoelectric absorption for biologic tissues is relatively small compared with Compton scattering, which is the dominant interaction process. For the potentiality to become a reality, the scattered photon must be detected and also must fall within the energy acceptance window that generally is set according to the energy resolution of the scintillation detectors used. An important difference exists between Compton scatter in single-photon emission CT and PET. In the former, scattered and unscattered LoRs cannot be formed outside the body and carry information that can be useful for determination of the body outline or of the non-uniform attenuation map [11–13]. In PET, however, scattered LoRs sometimes are formed outside the body and/or outside the imaging FoV, as discussed earlier.

In activity quantification, attenuation and scatter have opposite effects on the activity estimate. The rationale is that attenuation tends to decrease the number of detected counts, thus reducing the activity estimate, whereas Compton scatter tends to increase the number of detected counts, thus overestimating the activity. Both result in a loss of contrast and amplify quantitative errors or bias. The trend in nuclear medicine has been to correct for Compton scatter and for attenuation independently and in that order. This trend is driven by the desire to separate the complex compensation problem of two interrelated processes into two simpler components. In some sense, this situation is analogous to conventional two-dimensional (2D) reconstruction versus fully 3D reconstruction, which considers oblique LoRs. Taking advantage of the 3D acquisition mode increases the sensitivity by approximately a factor of five compared with the 2D acquisition mode. This advantage, however, is achieved at the expense of an increased system sensitivity to random and scattered coincidences and the greater complexity and computational burden of the 3D reconstruction algorithm. Novel methods of handling scatter and attenuation simultaneously

have many advantages over conventional correction methods. The most ambitious approaches aiming to achieve combined corrections, originally referred to as “inverse Monte Carlo” simulations [14], endeavor to reconstruct Compton-scattered photons into their voxel of origin. These approaches, which are discussed in a later section, seem to be too ambitious to be feasible in a clinical setting [15–19]. More realistic approaches include both attenuation and scatter in the forward projection operator of an iterative reconstruction algorithm (eg, maximum-likelihood expectation maximization, ML-EM), in which only unscattered photons are “put back” [20–23].

The magnitude of the included scatter in PET depends heavily on the acquisition mode, the placement and width of the energy acceptance window, the body section being imaged (eg, brain, thorax, abdomen, or pelvis), and patient size. The mode depends on whether the FoV for a given detector

is restricted in the axial direction (along the patient axis) by the placement of lead or tungsten septa (2D mode) or is left considerably more open (3D mode). For standard energy window settings, the scatter fraction—defined as the ratio between the number of scattered photons and the total number of photons (scattered and unscattered) detected—represents 10% to 20% of the total counts acquired in the 2D mode, whereas in the 3D mode it increases to 30% to 35% of the data collected in brain scanning and can reach 50% to 60% of the data collected in whole-body scanning (Fig. 2) [2,24]. It has been demonstrated that in the 3D acquisition mode, the variation of the scatter fraction as a function of the phantom size is not linear, reaching a maximum of 66% for a point source located in the center of a cylindrical phantom (diameter 50 cm, height 20 cm) [25]. The scatter fraction for the same point source in air is higher in the 2D mode (6%) than in the 3D mode (2%) because of

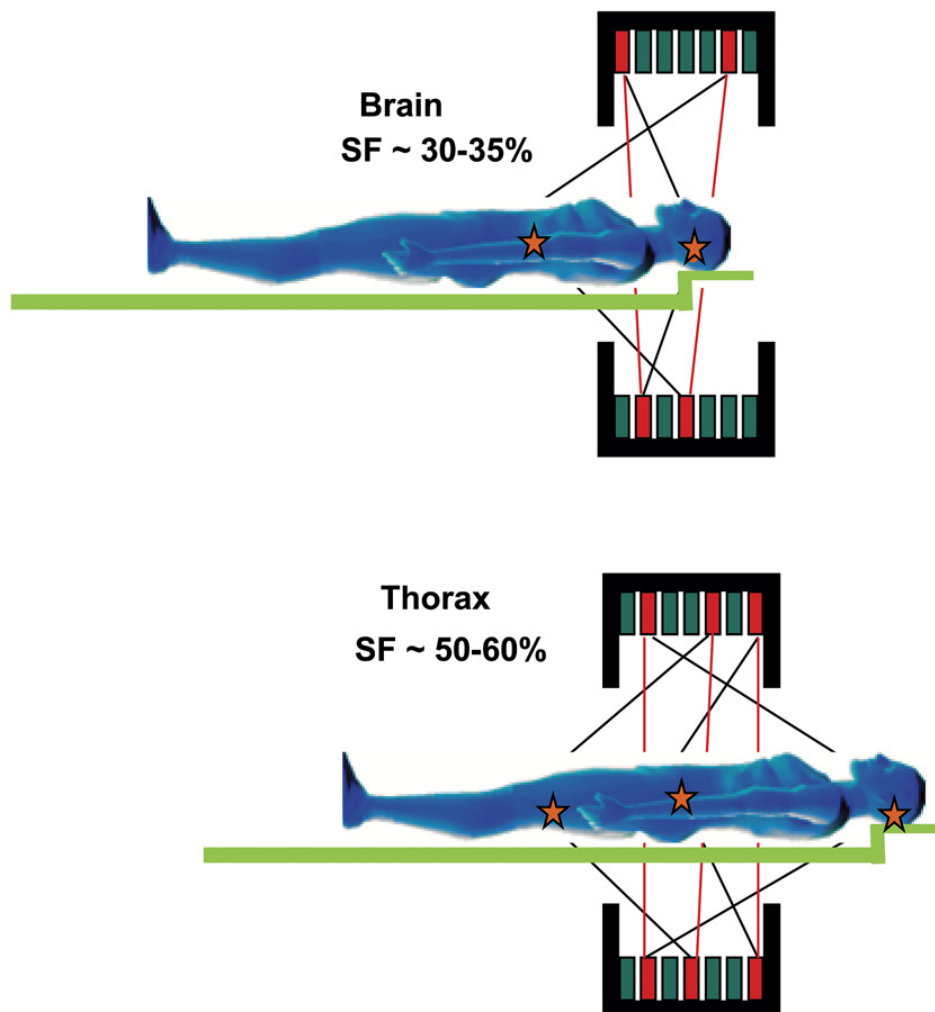


**Fig. 2.** Scattered photons arise from the whole attenuating medium, including the imaging table and the various components of a PET tomograph. The scatter fraction in PET in the 3D mode ranges from 30% to 35% of the data acquired in brain scanning to more than 50% of the data acquired in whole-body scanning, depending on the scanner geometry, the energy window setting, the region to be explored, and patient size. In addition to a decrease in the image contrast, events also may appear in regions of the image where there is no activity (eg, outside the patient).

the contribution of scatter in the septa in the 2D mode. Another concern in 3D PET, in contrast to 2D PET, is the scatter contribution from activity outside the FoV and the contribution of multiple scatter.

The scientific literature lacks thorough studies focusing on the clinical impact of different scatter-correction strategies versus no correction in 3D PET imaging. It is well established that scatter correction improves the contrast compared with no correction but does so at the expense of decreased signal-to-noise ratio when subtraction-based scatter-correction techniques are used [26]. Scatter compensation improves the contrast between the different brain tissues and removes background counts in the abdomen and lungs, allowing better recovery of tracer-avid or low-count regions and structures [2]. The value of scatter compensation is well established within the PET community, both for optimal qualitative assessment of reconstructed images and for quantification of parameters governing physiologic and biologic processes.

There are still, however, some applications in which the benefit of scatter correction remains controversial. These applications include  $^{15}\text{O}$ -[H<sub>2</sub>O]-based brain-activation protocols that are characterized by low-count studies in which scatter subtraction enhances noise, thus jeopardizing the power of statistical analysis. The goal of these studies is to identify functional differences between subjects scanned under different conditions (ie, baseline and following an activation task). Whether the scatter component in the two conditions can be considered as a constant for intersubject comparisons still needs to be demonstrated. This constancy is needed to substantiate the hypothesis that the outcome of statistical analysis (reflecting subtle changes in radiotracer distribution) does not change significantly before and after scatter correction.

In tracer kinetic modeling studies, differences ranging from 10% to 30% in the parameter estimates derived from patient studies are often found to be significant [27]. The magnitude of the scatter correction may cause some parameter values to increase by several fold, with an associated increase in noise. The use of subtraction-based scatter correction might jeopardize the ability to detect slight biologic effects if the decrease in signal-to-noise ratio cannot be circumvented. Very few studies have addressed the issue of the effect of scatter compensation on parameter estimates derived from kinetic models that focused mainly on 3D brain PET studies [27,28]. Further studies using different PET tracers in various clinical situations are necessary to characterize fully the effect of scatter correction on the estimation of tracer kinetic parameters.

### Modeling the scatter component in uniform and non-uniform media

The transport of annihilation photons is described by the integro-differential Boltzmann equation, which is the governing equation for a given monoenergetic, isotropic source of photons and a scattering medium. The differential part describes the generation, propagation, and attenuation of photons. The integral part describes the scattering of photons as an integral over direction and energy. The Boltzmann equation describes the evolution of the spatial and angular distribution of photons with respect to time resulting from the generation, propagation, attenuation, and scattering of photons within the medium. This equation is difficult to solve because of the scatter integral and the size of the problem when discretized. Many techniques deal with the scatter integral by considering successive orders of scattering discretely.

The probability of Compton scattering is given by the Klein-Nishina equation, which gives the differential scattering cross section  $d\sigma/d\Omega$  as a function of scattering angle  $\theta$  [29]:

$$\frac{d\sigma}{d\Omega} = \frac{r_e^2}{2} (1 + \cos^2\theta) \left[ \frac{1}{1 + \alpha(1 - \cos\theta)} \right]^2 \left[ 1 + \frac{\alpha^2 (1 - \cos\theta)^2}{[1 + \alpha(1 - \cos\theta)] (1 + \cos^2\theta)} \right]$$

where  $\alpha = E/m_0c^2$  and  $r_e$  the classical radius of the electron. This equation was used extensively to build appropriate scatter models to correct for this effect in PET. Because all unscattered events in PET have 511 keV before scattering,  $\alpha = 1$  for the first scatter. Therefore, the differential Compton scattering cross section relative to that for unscattered annihilation photons is

$$\frac{d\sigma}{d\Omega} = \frac{r_e^2}{2} \left[ \frac{1}{(2 - \cos\theta)^2} \right] \left[ 1 + \cos^2\theta + \frac{(1 - \cos\theta)^2}{(2 - \cos\theta)} \right]$$

This equation gives the differential scattering probability. The integral of this from 0° to any angle gives the integral cross section. The integral gives information about what fraction of scattered photons will be scattered into a cone with a given half-angle. The theoretic angular and energy distributions of Compton-scattered photons are plotted as a function of the scattering angle and energy in Fig. 3A and B, respectively, for an initial energy of 511 keV. The figure shows that small-angle scattering is more likely than large-angle scattering and that the most probable scattering angle is around 35°. The corresponding energy of the Compton-scattered photon is about 433 keV, which is within

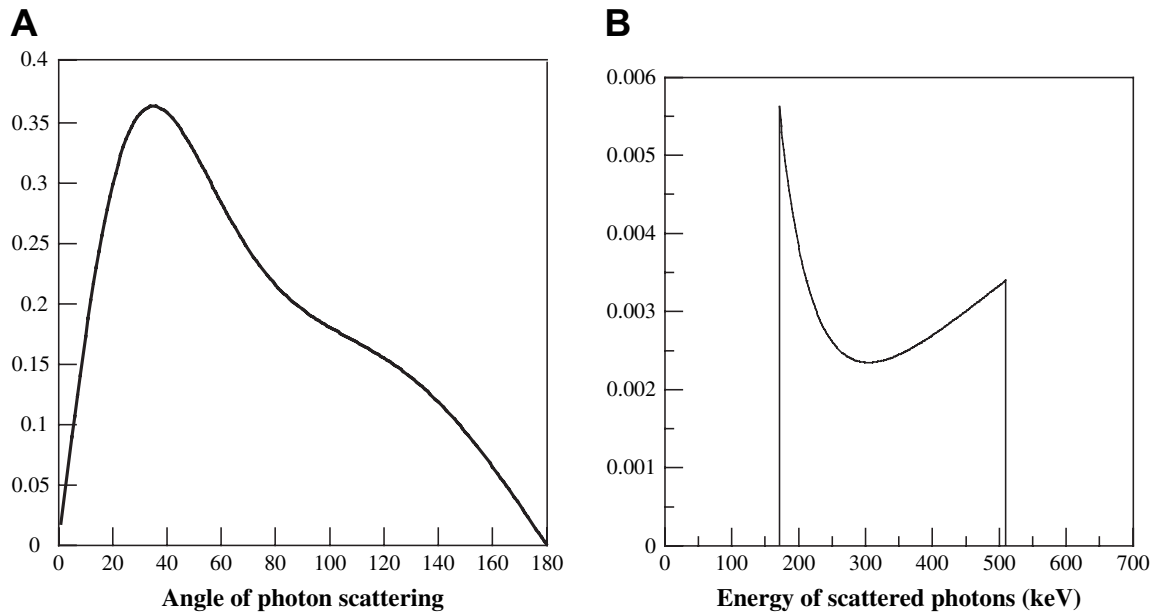


**Fig. 3.** The theoretic (A) angular and (B) energy distributions of Compton single-scattered photons having an initial energy of 511 keV, according to the Klein-Nishina expression.

the acquisition energy window used on most current, state-of-the-art PET scanners.

The process of modeling the scatter component in PET consists of creating a representation of the scatter counts (magnitude and spatial distribution) in a projection or sinogram that corresponds to a particular tracer activity distribution and attenuation map in the object [2]. The ideal research tool for scatter modeling through accurate photon transport is the Monte Carlo method [1]. The complexity and computing requirements of Monte Carlo simulations led to the development of analytic models based on the integration of the Klein-Nishina equation or simplifying approximations to improve computational speed, particularly in media of non-uniform density. Analytic scatter modeling in uniformly attenuating objects is more straightforward and usually has been performed by scanning point or line sources placed at various locations in a water-filled cylinder as a first step toward modeling scatter from multiple and distributed sources within non-uniform scattering media using anatomy-dependent models. Point- or line-spread scatter-response functions are generated, and the scatter fraction is assessed by fitting the scatter tails of the response function to an appropriate mathematical expression (eg, Gaussian, mono- or dual-exponential kernels). This approach was performed extensively by Barney and colleagues [30] during the early days of fully 3D PET imaging to develop and validate an analytic scatter model that can be used for scatter correction. Likewise, Adam and colleagues [25] used Monte Carlo simulations to extend the assessment of the spatial characteristics of scatter to contributions from outside the FoV using

various phantoms. The spatial distribution of multiple scatter is quite different from the simple scatter component, preventing the use of simple rescaling of the latter to take into account the effect of the former for scatter-correction purposes. Fig. 4 shows Monte Carlo-simulated scatter distribution functions for a line source located at the center of the FoV and displaced 5 cm radially off center obtained using the Eidolon simulation package [31]. The projections for the line source at the center are symmetrical and were summed over all projection angles. The projections are not symmetric when the source is moved off center. For this reason, a profile of a single angular view was used. It can be seen that the projections of a line source placed in a uniform, water-filled cylinder are dominated in the wings by the object scatter and in the peak by the unscattered photons. This discussion remains valid when the line source is shifted out of the symmetry center. The amplitude of the short side of the projection compared with that of the symmetric case is increased, because the path of the photons through the phantom is shorter. The amplitude of the long side is decreased, because the pathway through the attenuating medium is longer.

Because of the limitations of Gaussian models, a new approach that allows the modeling of non-Gaussian object-dependent scatter was developed by Chen and colleagues [32]. Images of simple and more complex phantoms were used to derive the 24 parameters of the model, which consists of eight simple functions. The parameters for various objects were derived from those of a reference object consisting of a cylinder 21.5 cm in diameter, using empiric rules.

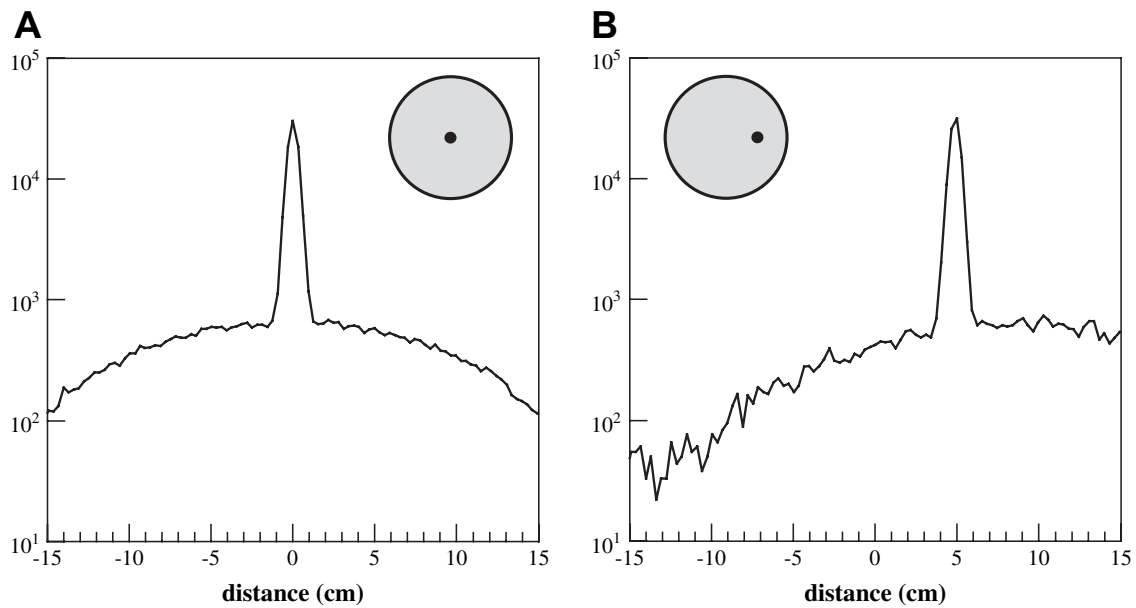


**Fig. 4.** The scatter-response functions simulated using Monte Carlo calculations when the line source is located at the center of the FOV (A) and displaced 5 cm radially (B). The projections for the line source at the center are symmetric and were summed over all projection angles.

The effect of lower energy discrimination on single- and multiple-scatter distributions was also assessed through Monte Carlo calculations for 3D PET using both a 45.6-cm (full object) and a 15.2-cm (short object) section of the VoxelMan anthropomorphic model [33]. Consistent with the observations made by Adam and colleagues [25], the multiple-scatter component was well estimated with a Gaussian convolution of the single-scatter events (for the full object), but significant errors may occur if the attenuation and activity outside the FoV are not included in the estimation of the single-scatter component. Using the same anthropomorphic model with the lungs and heart in the FoV and the abdomen outside the FoV, the scatter fraction was 57% and 36%, when using a low energy discrimination of 300 keV and 425 keV, respectively. Of the total scatter, 7.4% was found to come from outside-FoV matter and 24% from outside-FoV activity when using a low energy discrimination of 300 keV whereas they were only 5.3% and 17% when using a low energy discrimination of 425 keV. Moreover, the spatial distributions of scatter from external matter and external activity were found to be different [34]. More recently, a more sophisticated and promising approach that offers distinct features for modeling multiple-order Compton scatter, which uses the absolute probabilities relating the image space to the projection space in 3D whole-body PET, was proposed [35]. Such modeling is valuable for large, attenuating media in which scatter is a prevailing component of the measured data and in which multiple scatter may dominate the scatter component (depending on energy discrimination and object size).

Another category of methods uses analytic models or Monte Carlo simulations to compute the transition matrix, which represents the mapping from the activity distribution onto the projections. Monte Carlo simulation can handle complex activity distributions and non-uniform media readily [14,16,18,19]. Unfortunately, hundreds of gigabytes up to several terabytes of memory are required to store the complete nonsparse transition matrix when the fully 3D Monte Carlo matrix approach is used, and without approximations it can take several weeks to generate the full matrix on standard computing platforms. In addition, the procedure must be repeated for each patient. One of the advantages of such an approach is that the scatter model can be incorporated readily in direct 3D list-mode iterative reconstruction algorithms [36]. This advantage has spurred further research aiming at reducing memory constraints through the development of appropriate, parallelizable compression schemes to enable storing the matrices of the full Monte Carlo scatter system [37].

#### Scatter component in small-animal positron emission tomography imaging

With the introduction of commercial preclinical PET systems, small-animal imaging is becoming readily accessible and increasingly popular. Because in most cases the choice of a particular system is dictated by technical specifications, special attention must be paid to the methodologies followed when characterizing system performance. Because different methods can be used to assess the scatter fraction, differences may be methodologic rather

than reflecting any relevant difference in the performance of the scanner. Standardization of the assessment of performance characteristics is thus highly desired [38].

Little has been published on modeling the scatter component in small-animal PET scanners, because in imaging rodents the scatter fraction is relatively small (compared with clinical imaging). The origin of scatter for small-animal imaging has not been well characterized but has been proposed to stem mainly from the gantry and environment rather than from the animal itself [39]. The scatter component for a prototype PET scanner based on avalanche photodiode readout of two layers of lutetium oxyorthosilicate crystals with depth of interaction information (called the "Munich-Avalanche-Diode-PET" [MADPET]) was assessed using Monte Carlo calculations [40]. In the most advanced version of this prototype (MADPET-II), the scatter fraction in a mouse-like cylindrical phantom (6 cm in diameter, 7 cm in height) containing a spherical source (5 mm in diameter) placed at its center was 16.2% when the cylinder was cold and increased to 37.7% when the cylinder was radioactive for a lower energy discriminator of 100 keV and no restrictions in the acceptance angle [41]. Monte Carlo simulations showed that small-animal PET scanners also are sensitive to random and scattered coincidences from radioactivity outside the FoV [42].

Important contributions to the field were made by Bentourkia and colleagues [43] who used multispectral data acquisition on the Sherbrooke small-animal avalanche photodiode PET scanner to fit the spatial distribution of individual scatter components of the object, collimator, and detector using simple mono-exponential functions. The scatter fraction of this scanner for rat imaging was estimated as 33.8% with a dominant contribution by the single-scatter component (27%) as assessed by Monte Carlo calculations [44]. The position-dependent scatter parameters of each scatter component then are used to design nonstationary scatter-correction kernels for each point in the projection. These kernels are used in a convolution-subtraction method that consecutively removes object, collimator, and detector scatter from projections [45]. This technique served as the basis for the implementation of a spatially variant convolution-subtraction scatter-correction approach using dual-exponential scatter kernels on the Hamamatsu SHR-7700 animal PET scanner [46].

Exhaustive experimental measurements also were carried out to characterize the magnitude and origin of scattered radiation for the microPET II small-animal PET scanner [39]. It has been shown that for mouse scanning, the scatter from the gantry and room environment as measured with a line

source placed in air dominates over object scatter. The environmental scatter fraction increases rapidly as the lower energy discriminator decreases and can exceed 30% for an open energy window of 150 to 750 keV. The scatter fraction originating from the mouse phantom is very low (3%–4%) and does not change considerably when the lower energy discriminator is increased. The object-scatter fraction for the rat phantom varies between 10% and 35% for different energy windows and increases as the lower energy discriminator decreases.

Likewise, the measured scatter fractions for the mouse (rat) National Electrical Manufacturers Association count rate phantom in the microPET-R4 and the microPET—FOCUS-F120 were 14% (29%) and 12.3% (26.3%), respectively, when a low energy discrimination of 250 keV was used [47]. If the discriminator is increased to 350 keV, the scatter fraction drops to 8.3% (19.6%) and 8.2% (17.6%), respectively. Scatter correction thus is more important for rat scanning, whereas a large energy window (ie, 250–750 keV) would be more appropriate to increase system sensitivity when scanning small objects (eg, mouse brain).

Similar approaches were undertaken for positron emission mammography units, in which high spatial and contrast resolution and sensitivity are required for early detection of breast tumors, hence avoiding biopsy intervention. In this context, a scatter-correction method for a regularized list-mode ML-EM reconstruction algorithm was proposed [48]. The object-scatter component is modeled as additive Poisson random variant in the forward model of the reconstruction algorithm. The mean scatter sinogram, which needs to be estimated only once for each positron emission mammographic configuration, is estimated using lengthy Monte Carlo simulations.

### Scatter-correction strategies in positron emission tomography

During the last 2 decades various techniques have been proposed for reducing scatter-corrupting photons and the resulting degradation of image contrast and loss of quantitative accuracy in PET. The major disparity among the correction algorithms is the way in which the scatter component in the energy acquisition window is assessed. The most reliable method to estimate the real amount and spatial distribution of scatter in the image is accurate modeling of scatter formation to resolve the observed energy spectrum into its unscattered and scattered components. Scatter-compensation techniques can be optimized by examining how accurately a scatter-compensation algorithm estimates the amount and spatial distribution of scatter under



conditions where it can be measured accurately or otherwise independently determined.

A number of PET scatter-compensation algorithms have been proposed in the literature. Following the review by Zaidi and Koral [2], they fall into five broad categories: (1) hardware approaches using coarse septa or beam stoppers; (2) multiple-energy-window (spectral-analytic) approaches; (3) convolution/deconvolution-based approaches; (4) approaches based on direct estimation of scatter distribution; and (5) approaches based on statistical reconstruction.

The review by Zaidi and Koral [2] and chapters in other books [49–51] offer a thorough review of PET scatter-correction methods as of 2004. Readers interested in these techniques are referred to these references. This article focuses on the most recent techniques, suggested during the last few years, that were not covered in these reviews.

### ***Hardware approaches using coarse septa or beam stoppers***

In addition to empiric methods, in which the most obvious approach consists of shifting the detection window towards the high energies to reduce scatter events in the energy acquisition window, many hardware-based approaches have been proposed. Among these approaches is the use of coarse septa, which results in higher sensitivity than obtained with the conventional 2D acquisition mode using interslice septa but a lower scatter fraction than in the 3D acquisition mode without septa [52]. The scatter component is determined from acquired data for those LoRs that are intercepted by the coarse septa. The technique seems to deal relatively well with scatter from radioactivity outside the FoV.

A related method uses a beam-stopper device made of lead, which is placed around the patient to attenuate primary beams, thus making it possible to estimate the scatter component directly in the PET sinogram domain from those LoRs blocked by stoppers [53]. By assuming that the spatial distribution of scatter varies slowly, the scatter component can be recovered using the cubic-spline interpolation from the local measurements or through combination using the dual-energy-window technique [54]. The authors claim that the technique clearly outperforms the dual-energy window technique for scatter subtraction and allows effective removal of multiple scatter and scattering from outside the FoV.

### ***Multiple-energy-window (spectral) approaches***

The development of the 3D acquisition mode and the improvements in detector energy resolution in PET have allowed the implementation of scatter correction based on the analysis of energy spectra [55].

Interest in energy-based scatter-correction techniques has been revived with the introduction of list-mode data storage in commercial PET scanners, which stores the energy information for the photon pair. The basic assumption of multiple-energy-window methods is that, given a sufficient number of windows below and above the photopeak window, one can estimate either the complete energy spectrum of the scattered counts or at least the integral of that spectrum from the lower energy discriminator of the photopeak window to the upper energy discriminator of that window. These techniques usually put in additional information to get potentially more accurate results, with the objective of subtracting the scattered counts, pixel by pixel.

During recent years, a few such techniques have been proposed. The method suggested by Chen and colleagues [56] uses energy-dependent weights; the values of its two energies indicate the probability an event being a “true” event. These weights are obtained from a precomputed representative true-fraction table obtained by averaging Monte Carlo calculation estimates for a variety of activity and attenuation distributions representative of clinical situations. One of the advantages of the method is that it requires minimal computations and is attractive for practical use.

A more comprehensive energy-based scatter-correction approach was suggested more recently by Popescu and colleagues [57]. The technique exploits the noticeable dissimilarity between the energy spectra of the unscattered and the scattered photons and uses the complete energy information from the list-mode data to assess the distribution of the scattered events in the data space. In addition, energy-dependent weights that individualize the correction terms (scatter and randoms) for each coincidence event, depending on its position and energy information, are incorporated in an iterative ML-EM reconstruction algorithm. The method relies on a 2D detector energy-response model corresponding to four possible combinations of the state of detected events: (1) both photons unscattered; (2) the first photon scattered and the second not scattered; (3) the second photon scattered and the first photon not scattered; and (4) both photons scattered. The statistical model also allows the variation of scatter fraction with the energies of coincident photons for each position in the projection space to be estimated. The use of a model with four energy components is the key difference between this technique and previously proposed energy-based approaches.

### ***Approaches based on convolution or deconvolution***

The convolution- or deconvolution-based approaches used in PET estimate the distribution of

scatter from the coincidence data collected in the standard energy acquisition window. These approaches are older and, especially in their simplest forms, are used less frequently than newer, more promising methods; therefore a minimum amount of space is given to them here. As discussed earlier, a spatially variant convolution-subtraction scatter correction was developed for a Hamamatsu SHR-7700 animal PET scanner designed for studies of conscious monkeys [46]. The technique builds on the approach adopted by Bentourkia and Lecomte [45], but a dual-exponential scatter kernel that takes into account the Compton scatter both inside the object and in the gantry and detectors was adopted instead of using separate mono-exponential kernels. The innovation is that this technique was used for scatter correction of both PET emission and transmission data, allowing a more accurate estimate of attenuation coefficients in the transmission data. Correction of both data sets improved image contrast and quantitative accuracy, thus reducing the residual error to approximately 2% in water.

#### ***Approaches based on direct calculation of scatter distribution***

Approaches based on the direct calculation of scatter distribution assume that the distribution of scattered events can be estimated accurately from the information contained in either the emission data alone or in the combined emission and the transmission data. Although the approach has met with a high level of enthusiasm, the role and clinical feasibility of direct Monte Carlo-based scatter correction in PET still needs to be demonstrated [19,58–60]. To this end, combining the advantages of general-purpose Monte Carlo codes developed for high-energy physics applications to allow more accurate modeling of complex PET detector geometries and those of dedicated PET simulators for modeling voxel-based anthropomorphic computational models of the human anatomy might be beneficial [61].

Analytic model-based scatter-correction algorithms generally use both the PET emission and transmission scans and a mathematical model of the scanner incorporating the physics of Compton scattering in a forward calculation of the number of events for which one photon has undergone a Compton interaction. Techniques using this class of algorithms remain the most popular and the most widely used in clinical settings, because they were successfully implemented on software supplied by virtually all vendors [62–64]. Fig. 5 shows the working principle of a model-based simulation scatter-correction technique proposed originally by Watson [62]. The magnitude and spatial

distribution of Compton scatter is determined using preliminary PET emission and transmission images and the Klein-Nishina formulation (analytically or using Monte Carlo calculations). The calculation usually is simplified by assuming photons scatter only once; then multiple scatter is modeled using the single-scatter component. A grid of scatter points is applied to calculate scatter projections, which are subtracted from measured projections before reconstruction. The technique usually is performed iteratively. Various implementations of the single-scatter simulation technique have been reported in the literature [21,62–66]. The approach was improved further to scale the estimated scatter sinogram more appropriately to the measured data, allowing more reliable compensation of scatter from outside the FoV, and to address some issues specific to combined PET/CT scanners (eg, the problem of CT image truncation) [67].

Interest in scatter correction for PET scanners using time-of-flight (ToF) information [68] was revived with the renewed interest in this old technology, which now can be exploited to its full potential because of the availability of faster scintillation crystals. The rationale is that scatter-compensation techniques developed for conventional PET may not be adequate for ToF-PET, particularly those model-based techniques that simulate scatter contributions. The correction algorithm must take into account the time offsets of detected scattered photon pairs, because the variation of scatter contribution may depend on time offset in a different way than do unscattered coincidences. To this end, the single-scatter simulation technique was extended to support the reconstruction of list-mode PET data with ToF information to consider the case in which Compton scatter is discriminated according to its differential ToF [69] and to predict the variation of scatter as a function of ToF [70]. The approach by Werner and colleagues [70] was designed for incorporation into list-mode ToF reconstruction. The algorithm computes high-resolution scatter time distributions at 585-picosecond timing resolution (because important structure is visible in the time distributions at this timing resolution) and uses an alternative tail-fit-based scaling technique. Preliminary results seem to suggest that a ToF-dependent scatter-correction technique is essential to achieve the fast convergence expected from ToF reconstruction while preserving or improving quantitative accuracy. Watson [69] characterized discrepancies between ToF-dependent and non-ToF-dependent scatter components and reported good agreement between calculated and measured ToF-dependent scatter using phantom and clinical studies. The computational burden of this technique, however, is significantly higher (by

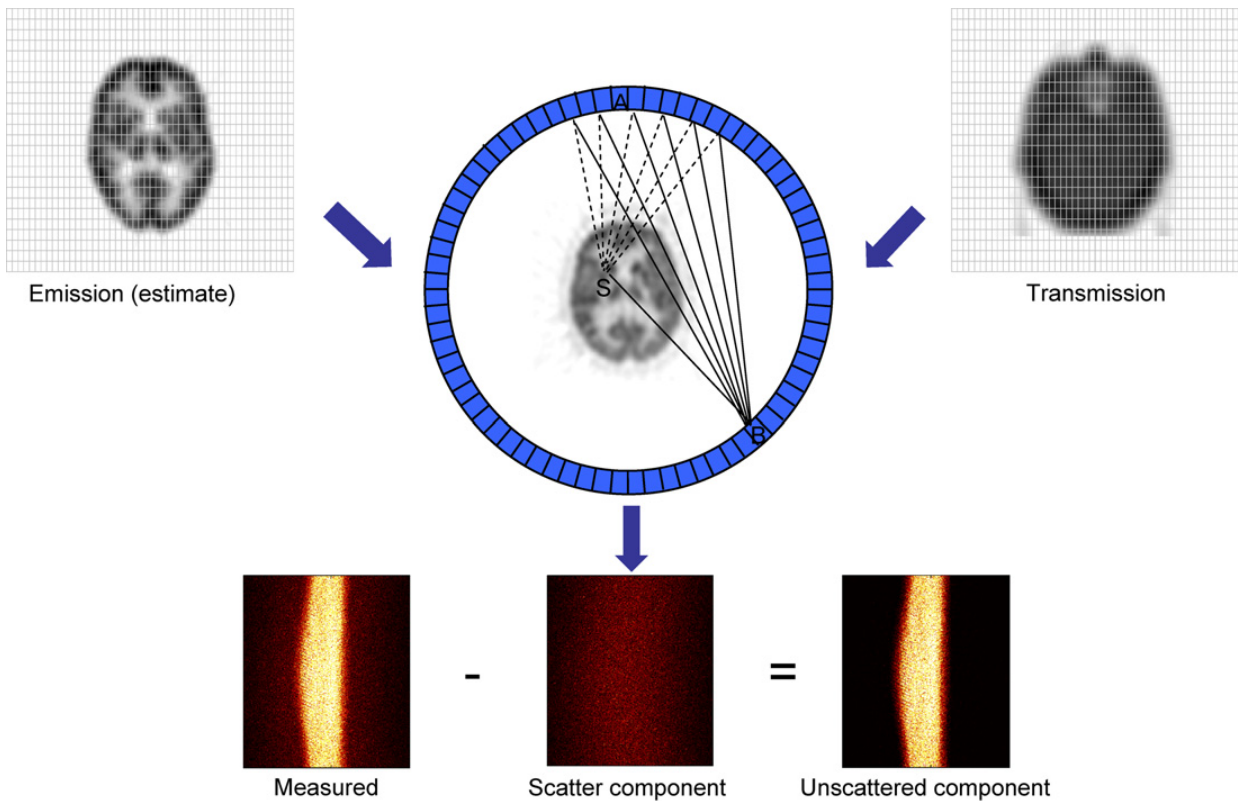


**Fig. 5.** Principle of model-based scatter-correction techniques. The magnitude and spatial distribution of Compton scatter is determined using preliminary PET emission and transmission images and the Klein-Nishina equation (analytically or using Monte Carlo calculations). Calculations usually are simplified by assuming photons scatter only once and then modeling multiple scatters using the single-scatter component. A grid of scatter points is applied to calculate scatter projections, which are subtracted from measured projections before reconstruction. The technique usually is performed iteratively.

a factor of five) than the initial non-ToF implementation of the algorithm.

### **Iterative reconstruction-based scatter-correction approaches**

The scatter component can be either precomputed (using one of the techniques described previously) and used during iterative reconstruction or can be generated as well as used during iterative reconstruction [71]. In the former approach the estimated scatter component is included with a forward projection in the statistical model instead of being explicitly subtracted from the measured projection data. That is, the goal of a given iteration becomes finding the object that, when it is forward projected and the scatter estimate is added, best fits the measured projection data, with “fit” quantified by the log-likelihood of the Poisson statistical model. In that model, the variance equals the mean, and the mean includes both the unscattered and scattered contributions [2].

The normal approach for implementation of a scatter model is to incorporate the scatter estimation directly in the transition matrix ( $a_{ij}$ ) of the ML-EM algorithm, in which case it becomes

considerably larger than when only attenuation and geometric factors are included. One class of correction methods uses Monte Carlo simulations to compute the complete transition matrix that represents the mapping from the activity distribution onto the projections [14–19], including scatter events. Compression schemes are being developed to alleviate memory constraints and to make numeric implementation on current state-of-the-art computing platforms feasible [37]. In most cases, the scatter estimate is added or subtracted as a constant term or is recalculated in the projector at each iteration and is not considered in the back-projector:

$$f_j^{new} = \frac{f_j^{old}}{\sum_l a_{lj}} \sum_i a_{ij} \frac{p_i}{\sum_k a_{ik} f_k^{old} + \hat{s}}$$

where  $p_i$  is the discrete set of projection pixel values,  $f_j^{new}$  and  $f_j^{old}$  refer to the current and previous estimates of the reconstructed object respectively, and  $(\hat{s})$  is the scatter estimated on all projections.

### **Comparison of methods**

The assessment and validation of scatter-correction algorithms is inherently difficult and sometimes is

unconvincing. There is a clear need for guidelines to evaluate correction techniques and other image-processing issues in PET. Most of the algorithms developed so far have been evaluated using either simulated or experimentally measured phantom studies, in addition to subjective visual interpretation of clinical studies followed by ranking performed by experienced physicians. This assessment has been extended to objective assessment of image quality using receiver operating characteristics analysis based on human or numeric observers [72], evaluation of the impact on the estimation of tracer kinetic parameters [27,28], and voxel-based statistical analysis in brain PET studies [73]. In the last instance, the impact of model-based scatter correction on the spatial distribution of  $^{18}\text{F}$ -labeled fluorodeoxyglucose ( $^{18}\text{F}$ -[FDG]) in reconstructed brain PET images of healthy subjects was assessed using statistical parametric mapping analysis. It has been shown that significant differences in  $^{18}\text{F}$ -[FDG] distribution arise when images are reconstructed with and without explicit scatter correction for some cerebral areas. Fig. 6 illustrates areas with significant changes in brain metabolism obtained by comparing distributions with and without explicit scatter correction, normalized using the same  $^{18}\text{F}$ -[FDG] template. The knowledge gained might help readers accustomed to interpreting non-scatter-corrected

images achieve adequate interpretation of  $^{18}\text{F}$ -[FDG] 3D brain PET images after scatter correction is applied.

In a clinical environment, the evaluation of scatter correction is hampered further by the multiplicity of medical purposes for which the corrections may be studied. There is no single figure of merit that summarizes algorithm performance, because performance ultimately depends on the diagnostic task being performed. Well-established figures of merit known to have a large influence on many types of task performance are generally used to assess image quality. Generally it is difficult to establish the superiority of one method over another. The impact of scatter correction on estimates of tracer kinetic parameters has been assessed in a few studies using brain FDG-PET data [27,28]. Further investigation using different tracers for various applications are necessary to characterize fully the effect of scatter correction on the estimation of tracer kinetic parameters.

A limited number of studies reported the comparative evaluation of different scatter-correction strategies in PET [28,59,60,74,75]. Most of the comparative evaluation studies concluded that virtually all correction methods improved the image contrast considerably compared with no correction but did so at the expense of a decrease in signal-to-noise ratio when using subtraction-based

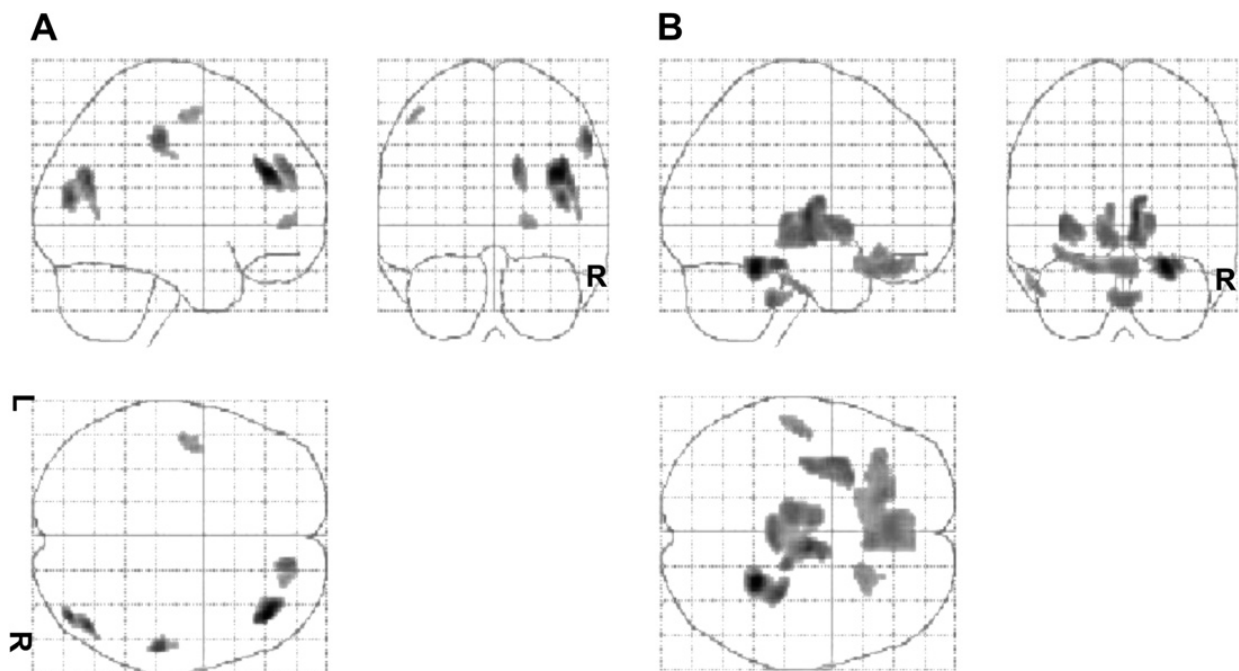


**Fig. 6.** Statistical parametric maps resulting from the comparison of images reconstructed using model-based scatter correction and those corrected for attenuation using an effective linear attenuation coefficient without explicit scatter correction normalized using the same  $^{18}\text{F}$ -[FDG] template showing (A) areas of significant regional decreases and (B) areas of significant regional increases in brain metabolism. (From Montandon M-L, Slosman DO, Zaidi H. Assessment of the impact of model-based scatter correction on  $^{18}\text{F}$ -[FDG] 3D brain PET in healthy subjects using statistical parametric mapping. *Neuroimage* 2003;20:1855; with permission.)

scatter-correction techniques. More importantly, some reports seem to suggest that the differences in the estimated scatter distributions did not have a significant impact on the final quantitative results. Thus, it can be argued that the important thing at present is to use some form of correction; future studies probably will ascertain the best method for a particular application.

### Scatter correction in transmission imaging

An issue that deserves special attention but has not been addressed sufficiently in the literature is the necessity for accurate modeling and correction of scatter in radionuclide transmission scanning, where the determined attenuation map generally is used for both attenuation and scatter-correction purposes, especially when using simultaneous emission/transmission scanning on standalone PET systems [76]. Some studies have reported the use of model-based approaches for scatter estimation in transmission imaging [77,78]. With the introduction and successful clinical implementation of dual-modality PET/CT systems, comparable approaches for scatter correction in x-ray CT imaging should be targeted for further research to allow the derivation of an appropriately scaled patient-specific attenuation map for correcting the PET emission data. This effect is more pronounced in the next generation of CT scanners with flat-panel, detector-based cone-beam configurations, which are much less immune to scatter than fan-beam CT scanners. In the past, in the context of using CT for quantitative measurements, different groups have addressed this problem by using experimental studies, mathematical modeling, and Monte Carlo simulations for both fan- [79–82] and cone-beam [83–88] (including flat-panel [89–95]) geometries. Pure Monte Carlo simulations and hybrid calculations (combining deterministic calculations and Monte Carlo simulations) will play a pivotal role in assisting these developments [96–98], because they also will help in the characterization of scatter resulting from the presence of additional material in future simultaneous PET/MR systems (eg, using field-cycled MRI technology [99]).

### Summary

It is gratifying to see the progress that scatter compensation has made in the last decade, from simple but practical energy-based approaches, through model-based strategies, and, more recently, iterative reconstruction-based approaches to scatter correction. Recent advances have been enormous, especially in improved accuracy, precision, and computational speed, in conjunction with

decreased calibration data. The need for scatter correction in PET is well accepted in research environments, where there is a greater emphasis on accurate quantitative measurements. Implementation of validated techniques in commercial software packages supplied by vendors would be useful to attract the interest of the clinical community. This greater interest, in turn, would lead to increased refinement of scatter-correction techniques. It is expected that, with the availability of greater computing power and more sophisticated tools through open-source software, more complex and ambitious computer-intensive scatter-modeling and -correction algorithms will become clinically feasible.

### References

- [1] Zaidi H. Relevance of accurate Monte Carlo modeling in nuclear medical imaging. *Med Phys* 1999;26:574–608.
- [2] Zaidi H, Koral KF. Scatter modelling and compensation in emission tomography. *Eur J Nucl Med Mol Imaging* 2004;31:761–82.
- [3] Links JM. Scattered photons as “good counts gone bad”: are they reformable or should they be permanently removed from society? *J Nucl Med* 1995;36:130–2.
- [4] Msaki P, Bentourkia M, Lecomte R. Scatter degradation and correction models for high-resolution PET. *J Nucl Med* 1996;37:2047–9.
- [5] Buvat I, Benali H, Todd-Pokropek A, et al. Scatter correction in scintigraphy: the state of the art. *Eur J Nucl Med* 1994;21:675–94.
- [6] Carlsson GA, Carlsson CA, Berggren KF, et al. Calculation of scattering cross sections for increased accuracy in diagnostic radiology. I. Energy broadening of Compton-scattered photons. *Med Phys* 1982;9:868–79.
- [7] Chelikani S, Gore J, Zubal G. Optimizing Compton camera geometries. *Phys Med Biol* 2004;49:1387–408.
- [8] Bailey DL. Data acquisition and performance characterization in PET. In: Valk PE, Bailey DL, Townsend DW, et al, editors. *Positron emission tomography: basic science and clinical practice*. 1st edition. London: Springer; 2003. p. 69–90.
- [9] Jaszczak RJ, Greer KL, Floyd CE, et al. Improved SPECT quantification using compensation for scattered photons. *J Nucl Med* 1984;25:893–900.
- [10] Blokland KJ, de Vos tot Nederveen Cappel WH, van Eck-Smit BL, et al. Scatter correction on its own increases image contrast in Tl-201 myocardium perfusion scintigraphy, but does it also improve diagnostic accuracy? *Ann Nucl Med* 2003;17:725–31.
- [11] Pan TS, King MA, Luo DS, et al. Estimation of attenuation maps from scatter and photopeak window single photon-emission computed tomographic images of technetium 99m-labeled sestamibi. *J Nucl Cardiol* 1997;4:42–51.

- [12] Truong T, Nguyen M, Zaidi H. The mathematical foundations of Compton scatter emission imaging. *Int J Biomed Imaging* 2007;1–11 (Article ID 92780, doi:10.1155/2007/92780).
- [13] Nguyen M, Truong T, Delarbre J, et al. Novel approach to stationary transmission scanning using Compton scattered radiation. *Phys Med Biol* 2007;52:4615–32.
- [14] Floyd CE, Jaszczak RJ, Greer KL, et al. Inverse Monte Carlo as a unified reconstruction algorithm for ECT. *J Nucl Med* 1986;27:1577–85.
- [15] Beekman FJ, de Jong HW, van Geloven S. Efficient fully 3-D iterative SPECT reconstruction with Monte Carlo-based scatter compensation. *IEEE Trans Med Imaging* 2002;21:867–77.
- [16] Rafecas M, Mosler B, Dietz M, et al. Use of a Monte Carlo-based probability matrix for 3-D iterative reconstruction of MADPET-II data. *IEEE Trans Nucl Sci* 2004;51:2597–605.
- [17] Cot A, Falcon C, Crespo C, et al. Absolute quantification in dopaminergic neurotransmission SPECT using a Monte Carlo-based scatter correction and fully 3-dimensional reconstruction. *J Nucl Med* 2005;46:1497–504.
- [18] Lazaro D, El Bitar Z, Breton V, et al. Fully 3D Monte Carlo reconstruction in SPECT: a feasibility study. *Phys Med Biol* 2005;50:3739–54.
- [19] Rehfeld N, Alber M. The influence of noise in full Monte Carlo ML-EM and dual matrix reconstructions in positron emission tomography. *Med Phys* 2006;33:3498–507.
- [20] Daube-Witherspoon ME, Carson RE, Yan YC, et al. Scatter correction in maximum-likelihood reconstruction of PET data. *Conference Record of IEEE Nuclear Science Symposium and Medical Imaging Conference* 1992;2:945–7.
- [21] Werling A, Bublitz O, Doll J, et al. Fast implementation of the single scatter simulation algorithm and its use in iterative image reconstruction of PET data. *Phys Med Biol* 2002;47:2947–60.
- [22] Tamal M, Reader AJ, Markiewicz PJ, et al. Noise properties of four strategies for incorporation of scatter and attenuation information in PET reconstruction using the EM-ML algorithm. *IEEE Trans Nucl Sci* 2006;53:2778–86.
- [23] Ponisch F, Enghardt W, Lauckner K. Attenuation and scatter correction for in-beam positron emission tomography monitoring of tumour irradiations with heavy ions. *Phys Med Biol* 2003;48:2419–36.
- [24] Schoder H, Erdi YE, Larson SM, et al. PET/CT: a new imaging technology in nuclear medicine. *Eur J Nucl Med Mol Imaging* 2003;30:1419–37.
- [25] Adam LE, Karp JS, Brix G. Investigation of scattered radiation in 3D whole-body positron emission tomography using Monte Carlo simulations. *Phys Med Biol* 1999;44:2879–95.
- [26] Barney JS, Harrop R, Atkins MS. Addition of noise by scatter correction methods in PVI. *IEEE Trans Nucl Sci* 1994;41:1551–5.
- [27] Cherry S, Huang SC. Effects of scatter on model parameter estimates in 3D PET studies of the human brain. *IEEE Trans Nucl Sci* 1995;42:1174–9.
- [28] Townsend D, Price J, Mintun M, et al. Scatter correction for brain receptor quantitation in 3D PET. In: Myers R, Cunningham V, Bailey DL, et al, editors. *Quantification of brain function using PET*. San Diego (CA): Academic Press; 1996. p. 76–81.
- [29] Klein O, Nishina Y. Über die Streuung von Strahlung durch freie Elektronen nach der neuen relativistischen Quantendynamik von Dirac. *Z Phys* 1929;52:853–68.
- [30] Barney JS, Rogers JG, Harrop R, et al. Object shape dependent scatter simulations for PET. *IEEE Trans Nucl Sci* 1991;38:719–25.
- [31] Zaidi H, Herrmann Scheurer A, Morel C. An object-oriented Monte Carlo simulator for 3D positron tomographs. *Comput Meth Prog Biomed* 1999;58:133–45.
- [32] Chen CH, Muzic RF Jr, Nelson AD, et al. A nonlinear spatially variant object-dependent system model for prediction of partial volume effects and scatter in PET. *IEEE Trans Med Imaging* 1998;17:214–27.
- [33] Lewellen TK, Harrison RL, Kohlmyer SG. Effect of lower energy threshold on single and multiple scatter distributions in positron volume imaging. *IEEE Trans Nucl Sci* 1999;46:1129–35.
- [34] Laymon CM, Harrison RL, Kohlmyer SG, et al. Characterization of single and multiple scatter from matter and activity distributions outside the FOV in 3-D PET. *IEEE Trans Nucl Sci* 2004;51:10–5.
- [35] Markiewicz PJ, Tamal M, Julyan PJ, et al. High accuracy multiple scatter modelling for 3D whole body PET. *Phys Med Biol* 2007;52:829–47.
- [36] Manavaki R, Reader AJ, Keller C, et al. Scatter modeling for 3-D PET list-mode EM reconstruction. *IEEE Nuclear Science Symposium Conference Record* 2002;3:1863–8.
- [37] Rehfeld N, Alber M. A parallelizable compression scheme for Monte Carlo scatter system matrices in PET image reconstruction. *Phys Med Biol* 2007;52:3421–37.
- [38] Weber S, Bauer A. Small animal PET: aspects of performance assessment. *Eur J Nucl Med Mol Imaging* 2004;31:1545–55.
- [39] Yang Y, Cherry SR. Observations regarding scatter fraction and NEC measurements for small animal PET. *IEEE Trans Nucl Sci* 2006;53:127–32.
- [40] Ziegler SI, Kuebler WK. Monte Carlo simulation of the scatter component in small animal positron volume-imaging devices. *Z Med Phys* 1993;3:83–7.
- [41] Rafecas M, Boning G, Pichler BJ, et al. A Monte Carlo study of high-resolution PET with granulated dual-layer detectors. *IEEE Trans Nucl Sci* 2001;48:1490–5.
- [42] Fulterer A, Schneider S, Gundlich B, et al. Scatter analysis of the ClearPET™ neuro using Monte Carlo simulations. *Advances in Medical*

- Engineering. Heidelberg (Germany): Springer Berlin Heidelberg; 2007. p. 109–14.
- [43] Bentourkia M, Msaki P, Cadorette J, et al. Assessment of scatter components in high-resolution PET: correction by nonstationary convolution subtraction. *J Nucl Med* 1995;36:121–30.
- [44] Bentourkia M, Laribi M, Lakinsky E, et al. Scatter restoration in PET imaging. *IEEE Nuclear Science Symposium Conference Record* 1992;2:1075–9.
- [45] Bentourkia M, Lecomte R. Energy dependence of nonstationary scatter subtraction-restoration in high resolution PET. *IEEE Trans Med Imaging* 1999;18:66–73.
- [46] Lubberink M, Kosugi T, Schneider H, et al. Nonstationary convolution subtraction scatter correction with a dual-exponential scatter kernel for the Hamamatsu SHR-7700 animal PET scanner. *Phys Med Biol* 2004;49:833–42.
- [47] Laforest R, Longford D, Siegel S, et al. Performance evaluation of the microPET®—FOCUS-F120. *IEEE Trans Nucl Sci* 2007;54:42–9.
- [48] Qi J, Huesman RH. Scatter correction for positron emission mammography. *Phys Med Biol* 2002;47:2759–71.
- [49] Bailey DL. Quantitative procedures in 3D PET. In: Bendriem B, Townsend DW, editors. *The theory and practice of 3D PET*. The Netherlands: Kluwer Academic Publishers; 1998. p. 55–109.
- [50] Meikle SR, Badawi RD. Quantitative techniques in positron emission tomography. In: Valk PE, Bailey DL, Townsend DW, et al, editors. *Positron emission tomography: basic science and clinical practice*. London: Springer; 2003. p. 115–46.
- [51] Zaidi H, Koral KF. Scatter correction strategies in emission tomography. In: Zaidi H, editor. *Quantitative analysis of nuclear medicine images*. New York: Springer; 2006. p. 205–35.
- [52] Hasegawa T, Tanaka E, Yamashita T, et al. A Monte Carlo simulation study on coarse septa for scatter correction in 3-D PET. *IEEE Trans Nucl Sci* 2002;49:2133–8.
- [53] Chuang K-S, Wu J, Jan M-L, et al. Novel scatter correction for three-dimensional positron emission tomography by use of a beam stopper device. *Nucl Instr Meth A* 2005;551:540–52.
- [54] Wu J, Chuang K-S, Hsu C-H, et al. Scatter correction for 3D PET using beam stoppers combined with dual-energy window acquisition: a feasibility study. *Phys Med Biol* 2005;50:4593–607.
- [55] Adam LE, Karp JS, Freifelder R. Energy-based scatter correction for 3-D PET scanners using NaI(Tl) detectors. *IEEE Trans Med Imaging* 2000;19:513–21.
- [56] Chen H-T, Kao C-M, Chen C-T. A fast, energy-dependent scatter reduction method for 3D PET imaging. *IEEE Nuclear Science Symposium Conference Record* 2003;4:2630–4.
- [57] Popescu LM, Lewitt RM, Matej S, et al. PET energy-based scatter estimation and image reconstruction with energy-dependent corrections. *Phys Med Biol* 2006;51:2919–37.
- [58] Levin CS, Dahlbom M, Hoffman EJ. A Monte Carlo correction for the effect of Compton scattering in 3-D PET brain imaging. *IEEE Trans Nucl Sci* 1995;42:1181–8.
- [59] Zaidi H. Comparative evaluation of scatter correction techniques in 3D positron emission tomography. *Eur J Nucl Med* 2000;27:1813–26.
- [60] Holdsworth CH, Badawi RD, Santos P, et al. Evaluation of a Monte Carlo scatter correction in clinical 3D PET. *Conference Record IEEE Nuclear Science Symposium* 2003;4:2540–4.
- [61] Barret O, Carpenter TA, Clark JC, et al. Monte Carlo simulation and scatter correction of the GE Advance PET scanner with SimSET and Geant4. *Phys Med Biol* 2005;50:4823–30.
- [62] Watson CC. New, faster, image-based scatter correction for 3D PET. *IEEE Trans Nucl Sci* 2000;47:1587–94.
- [63] Wollenweber SD. Parameterization of a model-based 3-D PET scatter correction. *IEEE Trans Nucl Sci* 2002;49:722–7.
- [64] Accorsi R, Adam L-E, Werner ME, et al. Optimization of a fully 3D single scatter simulation algorithm for 3D PET. *Phys Med Biol* 2004;49:2577–98.
- [65] Ollinger JM. Model-based scatter correction for fully 3D PET. *Phys Med Biol* 1996;41:153–76.
- [66] Tsoumpas C, Aguiar P, Ros D, et al. Scatter simulation including double scatter. *Conference Record of the IEEE Nuclear Science Symposium* 2005;3:5.
- [67] Watson CC, Casey ME, Michel C, et al. Advances in scatter correction for 3D PET/CT. *Conference Record of the IEEE Nuclear Science Symposium* 2004;5:3008–12.
- [68] Bendriem B, Soussaline F, Campagnolo R, et al. A technique for the correction of scattered radiation in a PET system using time-of-flight information. *J Comput Assist Tomogr* 1986;10:287–95.
- [69] Watson CC. Extension of single scatter simulation to scatter correction of time-of-flight PET. *Conference Record of the IEEE Nuclear Science Symposium* 2005;5:2492–6.
- [70] Werner ME, Surti S, Karp JS, et al. Implementation and evaluation of a 3D PET single scatter simulation with TOF modeling. *Conference Record of the IEEE Nuclear Science Symposium* 2006;3:1768–73.
- [71] Hutton B, Nuyts J, Zaidi H. Iterative image reconstruction methods. In: Zaidi H, editor. *Quantitative analysis in nuclear medicine imaging*. New York: Springer; 2006. p. 107–40.
- [72] Sankaran S, Frey EC, Gilland KL, et al. Optimum compensation method and filter cutoff frequency in myocardial SPECT: a human observer study. *J Nucl Med* 2002;43:432–8.
- [73] Montandon M-L, Slosman DO, Zaidi H. Assessment of the impact of model-based scatter correction on  $^{18}\text{F}$ -[FDG] 3D brain PET in healthy

- subjects using statistical parametric mapping. *Neuroimage* 2003;20:1848–56.
- [74] Sossi V, Oakes TR, Ruth TJ. A phantom study evaluating the quantitative aspect of 3D PET imaging of the brain. *Phys Med Biol* 1998;43:2615–30.
- [75] Castiglioni I, Cremonesi O, Gilardi M-C, et al. Scatter correction techniques in 3D PET: a Monte Carlo evaluation. *IEEE Trans Nucl Sci* 1999;46:2053–8.
- [76] Zaidi H, Hasegawa BH. Determination of the attenuation map in emission tomography. *J Nucl Med* 2003;44:291–315.
- [77] Digby WM, Hoffman EJ. An investigation of scatter in attenuation correction for PET. *IEEE Trans Nucl Sci* 1989;36:1038–42.
- [78] Wegmann K, Adam L-E, Livieratos L, et al. Investigation of the scatter contribution in single photon transmission measurements by means of Monte Carlo simulations. *IEEE Trans Nucl Sci* 1999;46:1184–90.
- [79] Joseph PM, Spital RD. The effects of scatter in x-ray computed tomography. *Med Phys* 1982;9:464–72.
- [80] Kanamori H, Nakamori N, Inoue K, et al. Effect of scattered x-ray on CT images. *Phys Med Biol* 1985;30:239–49.
- [81] Merritt RB, Chenery SG. Quantitative CT measurements: the effect of scatter acceptance and filter characteristics on the EMI 7070. *Phys Med Biol* 1986;31:55–63.
- [82] Ohnesorge B, Flohr T, Klingenbeck-Regn K. Efficient object scatter correction algorithm for third and fourth generation CT scanners. *Eur Radiol* 1999;9:563–9.
- [83] Endo M, Tsunoo T, Nakamori N, et al. Effect of scatter radiation on image noise in cone beam CT. *Med Phys* 2001;28:469–74.
- [84] Malusek A, Seger MM, Sandborg M, et al. Effect of scatter on reconstructed image quality in cone beam computed tomography: evaluation of a scatter-reduction optimisation function. *Radiat Prot Dosimetry* 2005;114:337–40.
- [85] Zbijewski W, Beekman FJ. Efficient Monte Carlo-based scatter artifact reduction in cone-beam micro-CT. *IEEE Trans Med Imaging* 2006;25:817–27.
- [86] Rinkel J, Gerfault L, Estève F, et al. A new method for x-ray scatter correction: first assessment on a cone-beam CT experimental setup. *Phys Med Biol* 2007;52:4633–52.
- [87] Endo M, Mori S, Tsunoo T, et al. Magnitude and effects of x-ray scatter in a 256-slice CT scanner. *Med Phys* 2006;33:3359–68.
- [88] Wiegert J, Bertram M, Rose G, et al. Model-based scatter correction for cone-beam computed tomography. *Proc SPIE* 5745:271–82.
- [89] Siewerdsen JH, Jaffray DA. Cone-beam computed tomography with flat-panel imager: magnitude and effects of x-ray scatter. *Med Phys* 2001;28:220–31.
- [90] Ning R, Tang X, Conover D. X-ray scatter correction algorithm for cone beam CT imaging. *Med Phys* 2004;31:1195–202.
- [91] Kyriakou Y, Kalender WA. X-ray scatter data for flat-panel detector CT. *Phys Med* 2007;23:3–15.
- [92] Zhu L, Bennett NR, Fahrig R. Scatter correction method for x-ray CT using primary modulation: Theory and preliminary results. *IEEE Trans Med Imaging* 2006;5:1573–87.
- [93] Siewerdsen JH, Daly MJ, Bakhtiar B, et al. A simple, direct method for x-ray scatter estimation and correction in digital radiography and cone-beam CT. *Med Phys* 2006;33:187–97.
- [94] Bertram M, Wiegert J, Rose G. Potential of software-based scatter corrections in cone-beam volume CT. *Proc SPIE* 2005;5745:259–70.
- [95] Ay M, Zaidi H. Assessment of errors caused by x-ray scatter and use of contrast medium when using CT-based attenuation correction in PET. *Eur J Nucl Med Mol Imaging* 2006;33:1301–13.
- [96] Ay M, Zaidi H. Development and validation of MCNP4C-based Monte Carlo simulator for fan- and cone-beam x-ray CT. *Phys Med Biol* 2005;50:4863–85.
- [97] Kyriakou Y, Riedel T, Kalender WA. Combining deterministic and Monte Carlo calculations for fast estimation of scatter intensities in CT. *Phys Med Biol* 2006;51:4567–86.
- [98] Zaidi H, Ay M. Current status and new horizons in Monte Carlo simulation of X-ray CT scanners. *Med Biol Eng Comput* 2007;45:809–17.
- [99] Handler WB, Gilbert KM, Peng H, et al. Simulation of scattering and attenuation of 511 keV photons in a combined PET/field-cycled MRI system. *Phys Med Biol* 2006;51:2479–91.